PROCEEDINGS OF SCIENCE

Transverse charge and magnetization densities: Improved chiral predictions down to $b = 1$ fm

Jose Manuel Alarcón

Theory Center, Jefferson Lab, Newport News, VA 23606, USA

Astrid N. Hiller Blin*

Institut für Kernphysik & PRISMA Cluster of Excellence, Johannes Gutenberg Universität, D-55099 Mainz, Germany

E-mail: hillerbl@uni-mainz.de

Manuel J. Vicente Vacas

Instituto de Física Corpuscular, Universidad de Valencia-CSIC, Institutos de Investigación, Ap. Correos 22085, E-46071 Valencia, Spain

Christian Weiss

Theory Center, Jefferson Lab, Newport News, VA 23606, USA

The transverse charge and magnetization densities provide insight into the nucleon's inner structure. In the periphery, the isovector components are clearly dominant, and can be computed in a model-independent way by means of a combination of chiral effective field theory (χEFT) and dispersion analysis. With a novel N/D method, we incorporate the pion electromagnetic form-factor data into the χEFT calculation, thus taking into account the pion-rescattering effects and ρ-meson pole. As a consequence, we are able to reliably compute the densities down to distances $b \sim 1$ fm, therefore achieving a dramatic improvement of the results compared to traditional χEFT calculations, while remaining predictive and having controlled uncertainties.

QCD Evolution 2017
22-26 May, 2017
Jefferson Lab Newport News, VA - USA

*Speaker.

PoS(QCDEV2017)052

1. Introduction

The study of the transverse charge and magnetization densities provides interesting insights into the baryon structure and strong interaction dynamics. The transverse densities are given by the two-dimensional Fourier transforms of the electromagnetic form factors and describe the distribution of charge and magnetzation at fixed light-front time, as appropriate for relativistic systems [1, 2, 3]. They are closely connected with the partonic description of nucleon structure in QCD and correspond to integrals of the impact parameter-dependent generalized parton distributions (GPDs) over the momentum fraction x.

Of particular interest are the transverse densities at peripheral distances $b = O(M_p i^{-1})$, since they are governed by chiral dynamics and can be computed model-independently using ChEFT [4, 5, 6]. This can be done naturally using a dispersive representation of the form factors, where they are expressed as integrals over their singularities in the timelike region (spectral functions), which correspond to hadronic exchanges between the nucleon and the current in the t-channel. The peripheral densities are governed by the lowest-mass hadronic exchange, which is the two-pion exchange (two-pion cut of the form factor). It was found that at transverse distances larger than $b \sim 3$ fm the electromagnetic densities are dominated by chiral dynamics and can be obtained from the ChEFT results for the spectral functions on the two-pion cut [7]. At smaller distances the densities are strongly affected by pion rescattering effects and the ρ-meson resonance in the $\pi\pi$ channel. In order to compute the peripheral densities down to distances $b \gtrsim 1$ fm these effects have to be included in the ChEFT calculation.

Here we report about a new method which includes $\pi\pi$ rescattering effects in the spectral functions and permits calculation of the peripheral densities down to distances $b \sim 1$ fm with controled uncertainties [8]. The method is based on elastic unitarity in the $\pi\pi$ system and uses an N/D method to separate the coupling of the $\pi\pi$ system to the nucleon from the $\pi\pi$ rescattering effects [8, 9, 10, 11]. ChEFT is used to calculate the coupling of the $\pi\pi$ system to the nucleon with controled accuracy, while the $\pi\pi$ rescattering effects are included through the empirical pion form factor. The method represents a great improvement compared to traditional ChEFT calculation of the spectral functions and has applications beyond the study of transverse densities [9, 10].

In the following, we describe the formalism used, focusing in particular on the dispersive improvement mentioned above, based on chiral unitarity and the pion form-factor data. We then show our results for the spectral functions and transverse densities of the nucleons, down to distances of $b = 1$ fm.

2. Formalism

The decomposition of the electromagnetic current for a nucleon N with mass m_N in terms of the Dirac $F_1(t)$ and Pauli $F_2(t)$ form factors is given as:

$$\langle N(p')|J^\mu|N(p)\rangle = \bar{u}(p')\left[\gamma^\mu F_1(t) + \frac{i\sigma^{\mu\nu}\Delta_\nu}{2m_N}F_2(t)\right]u(p), \tag{2.1}$$

with incoming and outgoing nucleon 4-momenta p and p', respectively, and corresponding Dirac spinors $u(p)$ and $\bar{u}(p')$. The 4-momentum transfer is denoted $\Delta = p' - p$, $t = \Delta^2$, and we use the usual definition of $\sigma^{\mu\nu} = (i/2)\,[\gamma^\mu, \gamma^\nu]$.

In the light-front form of relativistic dynamics [1, 2], at a fixed light-front time $x^+ = x^0 + x^3 = 0$ the 4-momentum transfer is purely transverse, $\boldsymbol{\Delta}_T$, and the form factors are represented as two-dimensional Fourier transforms of the transverse densities at the position $\boldsymbol{b}$,

$$F_i(t = -|\boldsymbol{\Delta}_T|^2) \;=\; \int d^2b\, e^{i\boldsymbol{\Delta}_T\cdot\boldsymbol{b}}\, \rho_i(b \equiv |\boldsymbol{b}|) \qquad (i = 1,2). \tag{2.2}$$

The transverse spatial distributions of charge and magnetization $\rho_1(b)$ and $\rho_2(b)$ are then invariant under boosts in the z-direction [3].

The baryon form factors are analytic functions of t and have a dispersive representation of the form

$$F_i(t) \;=\; \int_{t_{\rm thr}}^{\infty} \frac{dt'}{t' - t - i0}\, \frac{{\rm Im}\, F_i(t')}{\pi} \qquad (i = 1,2), \tag{2.3}$$

where $t_{\rm thr}$ is the threshold of the spectral functions. With Eqs. 2.2 and 2.3, the transverse densities are then connected to the spectral functions via the dispersive integrals [4, 12]

$$\rho_1(b) = \int_{t_{\rm thr}}^{\infty} dt\, \frac{K_0(\sqrt{t}b)}{2\pi}\, \frac{{\rm Im}F_1(t)}{\pi}, \tag{2.4}$$

$$\widetilde{\rho}_2(b) = -\int_{t_{\rm thr}}^{\infty} dt\, \frac{\sqrt{t}K_1(\sqrt{t}b)}{4\pi m_N}\, \frac{{\rm Im}F_2(t)}{\pi}, \tag{2.5}$$

where $K_n(z)$ $(n = 0, 1)$ denote the modified Bessel functions of the second kind. These integrals converge exponentially at large t and large b, leading to a suppression of higher-mass scales at the periphery. In this region, it is therefore sufficient to take into account the low-mass hadronic states, such as the two-pion and two-kaon cuts computed in χEFT. The details of this calculation can be found in Refs. [8, 13].

The χEFT expressions by themselves describe the nucleon isovector spectral functions only in the region close to the two-pion threshold, the kaon contributions being negligible. In order to extend the description to higher t, the strong pion rescattering has to be taken into account. This effect manifests itself in the t-channel ρ-meson exchange at $t \sim 0.6\,{\rm GeV}^2$.

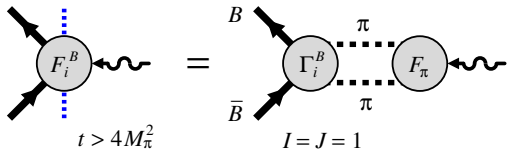

Figure 1: Unitarity relation for the isovector spectral function on the two-pion cut.

As is shown in Fig. 1, the nucleon isovector spectral function on the two-pion cut can be expressed as [14]

$${\rm Im}F_i(t) = \frac{k_{\rm cm}^3}{\sqrt{t}}\, \Gamma_i(t)\, F_\pi^*(t) = \frac{k_{\rm cm}^3}{\sqrt{t}}\, \frac{\Gamma_i(t)}{F_\pi(t)}\, |F_\pi(t)|^2 \qquad (i = 1,2), \tag{2.6}$$

where $k_{\rm cm} = \sqrt{t/4 - M_\pi^2}$ is the center-of-mass momentum of the two-pion system in the t-channel, $\Gamma_i(t)$ is the complex $I = J = 1$ $\pi\pi \to N\bar{N}$ partial-wave amplitude, and $F_\pi(t)$ is the complex pion

form factor in the timelike region. This follows from the unitarity condition in the t–channel and is valid strictly in the region up to the four-pion threshold. The pion form factor has a right-hand cut at the two-pion threshold, while the partial-wave amplitude has both this right-hand cut and a left-hand cut resulting from s-channel baryon exchanges. According to the Watson theorem [15], the complex functions $\Gamma_i(t)$ and $F_\pi(t)$ have the same phase on the two-pion cut, and therefore their ratio is real at $t > 4M_\pi^2$, also being free of pion-rescattering effects. The pion form factor $|F_\pi(t)|^2$ can be extracted directly from the $e^+e^- \to \pi^+\pi^-$ exclusive annihilation cross section, without the need of determining the phase of the complex form factor. Thus, the $\pi\pi \to N\bar{N}$ t-channel partial-wave amplitude is represented in the form $\Gamma_i(t) = N(t)/D(t)$, such that the right-hand cut (related to the t–channel exchanges) appears only in the factor $1/D(t) = F_\pi(t)$ [16], and the left-hand cut (related to the s-channel intermediate states) appears in the factor $N(t) = \Gamma_i(t)/F_\pi(t)$.

Within relativistic $SU(3)$ χEFT with the explicit inclusion of spin-3/2 degrees of freedom, we calculate the ratio $\Gamma_i(t)/F_\pi(t)$, dominated by the singularities of the nucleon Born graphs. It is not affected by pion-rescattering effects, consequently avoiding large higher-order χEFT corrections. We then multiply the result with the empirical pion form factor $|F_\pi(t)|^2$, containing the effects of pion rescattering, for which we use the Gounaris-Sakurai parametrization [17] with the parameters determined in Ref. [18].

Concerning the isoscalar spectral functions, they are dominated by the ω and ϕ-meson pole contributions. The model used for their inclusion is detailed in Ref. [8].

3. Discussion of the results

As can be seen in Fig. 2, the N/D prescription described in the previous section results in a remarkable improvement of the predictions for the nucleon spectral functions (red bands) when compared with those from traditional χEFT (blue bands). Figs. 2a and c show that the improved results agree well with those obtained from amplitude analyses via analytic continuation of the $\pi\pi \to N\bar{N}$ partial-wave amplitudes [19, 20] or Roy-Steiner equations [21]: the qualitative agreement is good in the whole region considered, and, in a leading-order calculation of the ratio $\Gamma_i(t)/F_\pi(t)$, we reproduce the amplitude-analysis results quantitatively up to $t \sim 0.3$ GeV^2 within errors. This is achieved even though no new free parameters are added, and the results continue being a genuine prediction of χEFT. Furthermore, it has been shown in Refs. [9, 10] that a next-to-next-to-leading order calculation of $\Gamma_i(t)/F_\pi(t)$ is sufficient to reproduce the results in the entire region up to $t \sim 0.8$ GeV^2.

The improvement has a dramatic effect on the peripheral transverse densities, as shown in Figs. 2b and d. At distances $b \sim 1$ fm, the predictions become up to an order of magnitude larger than in traditional χEFT approaches, and even at asymptotically large distances the improvement changes the densities by a constant factor of approximately 1.3. The densities decay exponentially at large b, as dictated by the analytic properties of Eqs. (2.4) and (2.5). At distances $b > 3$ fm, they are dominated by the isovector component, for which the dispersive improvement of the χEFT spectral functions performed in this work allows a predictive construction down to small distances $b \gtrsim 1$ fm. We show the decomposition into isovector and isoscalar components, $\{\rho^p, \rho^n\} = \rho^S \pm \rho^V$ in Fig. 3.

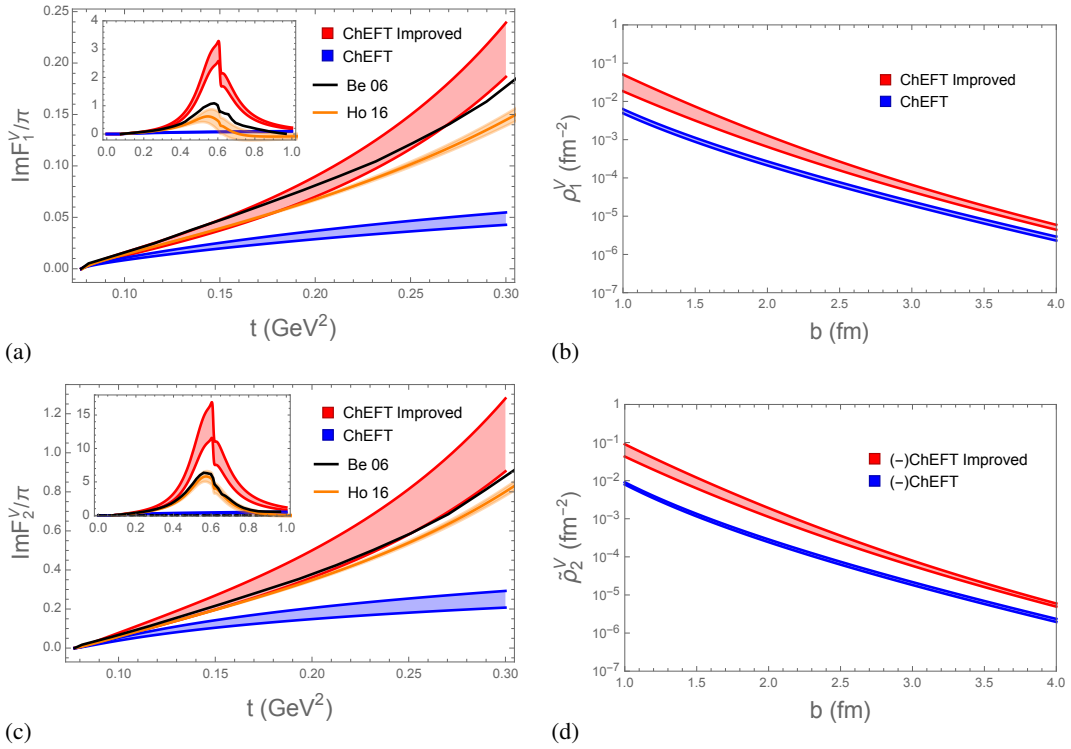

Figure 2: (a, c) Nucleon isovector spectral functions: the blue bands correspond to the χEFT results; the red bands are the results after improvement through unitarity; the brown bands and black line are the spectral functions obtained from Roy-Steiner equations [21] and the analytic continuation of the $\pi\pi \to N\bar{N}$ amplitudes [20, 19], respectively. The main plot shows the functions up to $t = 0.3\,\mathrm{GeV}^2$; the inset shows them up to $t = 1\,\mathrm{GeV}^2$. (b, d) Nucleon peripheral transverse isovector densities. The magnetic density is shown with opposite sign $(-)$ on the logarithmic scale.

For the proton, the charge density's isovector and isoscalar contributions have the same sign, leading to a positive total density with smooth behavior. For the neutron, on the other hand, the isovector and isoscalar components contribute with opposite sign, leading to cancellations in the total density. While in the periphery the neutron charge density is therefore negative, the results might be consistent with a positive charge density towards the center. However, the uncertainties in this region are too large to be able to make a definitive statement. The isoscalar component of the magnetization density is significantly smaller than in the charge density. As a result, the isovector magnetization density dominates down to much smaller distances $b \sim 1$ fm, and the proton and neutron have approximately opposite magnetization densities with smaller uncertainties in the whole region studied.

It is interesting to also inspect the quark flavor decomposition of the transverse charge and magnetization densities [12]:

$$\rho \;=\; e_u\rho^u + e_d\rho^d + e_s\rho^s \qquad (i=1,2), \tag{3.1}$$

where $\rho^f(b)$ $(f = u,d,s)$ represent the densities associated with the vector currents of the quark fields with flavor f. In order to study the relative contribution of the various quark flavors to the

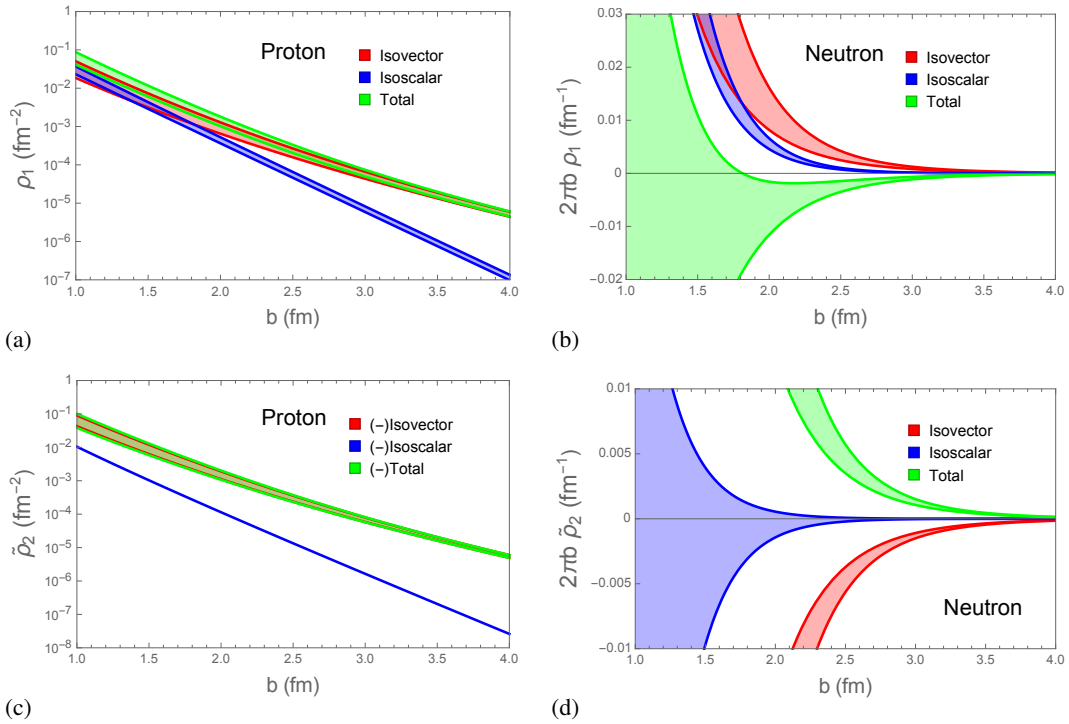

Figure 3: Transverse charge and magnetic densities of the nucleons. The red band shows the isovector component calculated using χEFT and dispersive improvement, while the blue band includes the vector-meson pole contrinbutions to the isoscalar component. The total density is shown in green.

charge density at a given distance, it is convenient to consider the ratios

$$R^f(b) \equiv= \frac{e_f \rho_1^f(b)}{\rho_1(b)}, \tag{3.2}$$

which at any b satisfy

$$\sum_f R^f(b) = 1, \tag{3.3}$$

and describe how the charge density at a given distance is decomposed into its quark flavor contributions. Its varition with b is slow due to the cancellation of the exponential factors.

In Fig. 4, the ratios calculated with the above introduced methods are shown for the proton. There are several aspects of interest to be outlined: at large distances $b > 3\,\text{fm}$ the u and d ratios approach the values $R^u = 2/3$ and $R^d = 1/3$, which are in accordance with u and d quark densities of equal magnitude and opposite sign. This points to the dominant pion-cloud contribution in the periphery. Even though the central regions in our calculations are provided with less accuracy than those of the periphery, we do obtain u and d ratios comparable with the number of u and d valence quarks at distances of $b \sim 1$ fm. This agrees with a mean-field picture of the motion of valence quarks in the nucleon [12]. On the other hand, the strange quark fraction is negligible in most of the region considered.

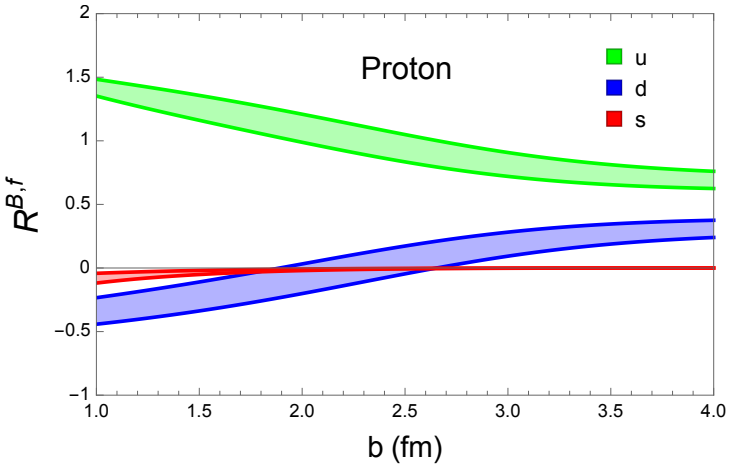

(a)

Figure 4: The ratios $R^f(b)$ $(f = u,d,s)$ (denoted $R^{B,f}(b)$ in the figure), Eq. (3.2), describing the relative contribution of each flavor to the total proton charge density at a given distance b.

4. Summary and conclusions

In this work, we gave predictions for the nucleon peripheral transverse charge and magnetic densities. We used a method of dispersive improvement of the isovector form factors in order to include the effects of pion rescattering and the ρ-meson pole. This is achieved by means of an N/D method that effectively separates the amplitude into a piece free of pion-rescattering effects, which can be calculated in χEFT, and a piece containing the pion-rescattering effects, which is represented by the empirical pion form factor.

This results in a major improvement of the form factors in the whole region considered, enabling a reproduction of results obtained from amplitude analysis. Furthermore, the isovector densities are enhanced by an order of magnitude in the the region of $b \sim 1$ fm, and slightly less drastically so towards the periphery. We conclude the pion-rescattering effects are essential for a reliable description not only of the central regions, but also for the nucleon periphery.

In the future, the methods presented here can be applied to a large variety of studies, such as the $\Delta(1232)$ transverse densities and nucleon–$\Delta(1232)$ transition form factors. In fact, while in the present work we considered the vector form factors, the method can also be extended to the study of baryon scalar form factors or those related to the strange current. Lastly, with the methods employed here, it would be interesting to study also the GPDs, connected to the transverse densities as described in Refs. [5, 6].

Acknowledgements

This material is based upon work supported by the U.S. Department of Energy, Office of Science, Office of Nuclear Physics under contract DE-AC05-06OR23177, and by the Deutsche

Forschungsgemeinschaft DFG. It was also funded by MINECO (Spain) and the ERDF (European Commission) grants No. FIS2014-51948-C2-2-P and SEV-2014-0398, and by the Generalitat Valenciana under Contract PROMETEOII/2014/0068.

References

[1] P. A. M. Dirac, Rev. Mod. Phys. **21**, 392 (1949) doi:10.1103/RevModPhys.21.392

[2] S. J. Brodsky, H. C. Pauli and S. S. Pinsky, Phys. Rept. **301**, 299 (1998) doi:10.1016/S0370-1573(97)00089-6 [hep-ph/9705477].

[3] M. Burkardt, Phys. Rev. D **62**, 071503 (2000) Erratum: [Phys. Rev. D **66**, 119903 (2002)] doi:10.1103/PhysRevD.62.071503, 10.1103/PhysRevD.66.119903 [hep-ph/0005108].

[4] M. Strikman and C. Weiss, Phys. Rev. C **82**, 042201 (2010) doi:10.1103/PhysRevC.82.042201 [arXiv:1004.3535 [hep-ph]].

[5] C. Granados and C. Weiss, JHEP **1507**, 170 (2015) doi:10.1007/JHEP07(2015)170 [arXiv:1503.04839 [hep-ph]].

[6] C. Granados and C. Weiss, JHEP **1606**, 075 (2016) doi:10.1007/JHEP06(2016)075 [arXiv:1603.08881 [hep-ph]].

[7] J. Gasser and H. Leutwyler, Annals Phys. **158**, 142 (1984) doi:10.1016/0003-4916(84)90242-2

[8] J. M. Alarcón, A. N. Hiller Blin, M. J. Vicente Vacas and C. Weiss, Nucl. Phys. A **964** 18 (2017) doi:10.1016/j.nuclphysa.2017.05.002 [arXiv:1703.04534 [hep-ph]].

[9] J. M. Alarcón and C. Weiss, Phys. Rev. C **96** no.5, 055206 (2017) doi:10.1103/PhysRevC.96.055206 [arXiv:1707.07682 [hep-ph]].

[10] J. M. Alarcón and C. Weiss, arXiv:1710.06430 [hep-ph].

[11] C. Granados, S. Leupold and E. Perotti, Eur. Phys. J. A **53** no. 6, 117 (2017) doi:10.1140/epja/i2017-12324-4 [arXiv:1701.09130 [hep-ph]].

[12] G. A. Miller, M. Strikman and C. Weiss, Phys. Rev. C **84**, 045205 (2011) doi:10.1103/PhysRevC.84.045205 [arXiv:1105.6364 [hep-ph]].

[13] A. N. Hiller Blin, Phys. Rev. D **96**, no. 9, 093008 (2017) doi:10.1103/PhysRevD.96.093008 [arXiv:1707.02255 [hep-ph]].

[14] W. R. Frazer and J. R. Fulco, Phys. Rev. **117**, 1603 (1960) doi:10.1103/PhysRev.117.1603

[15] K. M. Watson, Phys. Rev. **95**, 228 (1954) doi:10.1103/PhysRev.95.228

[16] G. Hohler and E. Pietarinen, Nucl. Phys. B **95**, 210 (1975). doi:10.1016/0550-3213(75)90042-5

[17] G. J. Gounaris and J. J. Sakurai, Phys. Rev. Lett. **21**, 244 (1968) doi:10.1103/PhysRevLett.21.244

[18] I. T. Lorenz, H.-W. Hammer and U. G. Meissner, Eur. Phys. J. A **48**, 151 (2012) doi:10.1140/epja/i2012-12151-1 [arXiv:1205.6628 [hep-ph]].

[19] G. Hohler, E. Pietarinen, I. Sabba Stefanescu, F. Borkowski, G. G. Simon, V. H. Walther and R. D. Wendling, Nucl. Phys. B **114**, 505 (1976). doi:10.1016/0550-3213(76)90449-1

[20] M. A. Belushkin, H.-W. Hammer and U. G. Meissner, Phys. Lett. B **633**, 507 (2006) doi:10.1016/j.physletb.2005.12.053 [hep-ph/0510382].

[21] M. Hoferichter, B. Kubis, J. Ruiz de Elvira, H.-W. Hammer and U.-G. MeiSSner, Eur. Phys. J. A **52**, no. 11, 331 (2016) doi:10.1140/epja/i2016-16331-7 [arXiv:1609.06722 [hep-ph]].